JOURNAL OF MATERIALS SCIENCE 21 (1986) 1932–1938

A model of the high-temperature deformation of metallic materials with ellipsoidal second-phase particles

M. TANAKA, H. IIZUKA
Department of Mechanical Engineering for Production, Mining College, Akita University, 1-1, Tegatagakuen-cho, Akita 010, Japan

A micromechanics model developed in the previous work which incorporated the effect of dynamic recovery by diffusion of atoms was applied to the interpretation of the high-temperature deformation of metallic materials with ellipsoidal second-phase particles. A theoretical discussion based on this model was made on the effect of several factors including shape, particle size, orientation and elastic modulus of second phase on the work-hardening behaviour of the materials at high temperature. A good correlation was found between the result of the calculations and those of the experiments obtained by the present authors or other investigators of several kinds of metallic materials with ellipsoidal second-phase particles. The dynamic recovery model used in this study can be applied to the understanding of high-temperature deformation behaviour or to the prediction of the possible recovery mechanism of the materials.

1. Introduction

The dispersion strengthening in metallic materials is strongly affected by several factors including volume fraction, shape, particle size, orientation and rigidity of second phase. Tanaka and Mori [1] discussed the work-hardening behaviour of a material with a disc-like, spherical or needle-like inclusion, using Eshelby's equivalent inclusion method [2]. Recently, Mori and Tokushige [3] and Matsuura [4] separately investigated the static and dynamic recovery of metals strengthened by spherical second-phase particles, based on the analysis of the climbing motion of misfit dislocations at the interface of a particle, which were introduced by plastic deformation of the matrix phase. The climbing rate of those dislocations at the interface can be affected by size, shape and orientation of second-phase particles in the recovery process at high temperature. However, the climb process of those dislocations is very complicated due to the interaction between the dislocations in each slip system. Therefore, it is difficult to know the effect of dynamic recovery from each dislocation motion alone.

Ashby [5] considered the static recovery of a dispersion-hardened metal, using a continuum mechanics model in which the recovery by diffusion of atoms is taken into account. It is obvious in the recovery process that atoms tend to migrate in the direction to diminish the misfit between second-phase particle and matrix (i.e. in the direction to decrease the elastic strain energy of second-phase particles and matrix). Therefore, the effect of dynamic recovery can be predicted to some extent by considering the average atom migration, even if the climbing motion of each dislocation is not known [6]. The authors revealed that the dynamic recovery of metallic materials with spherical precipitates can be explained by a micromechanics model [6] similar to that proposed by Ashby.

The effect of dynamic recovery on the work-hardening behaviour can depend on several factors such as size, shape and orientation of second-phase particles, difference in elastic moduli between second phase and matrix, as well as the rate-controlling mechanism which governs the recovery process. From both investigative and practical view points, it is important to know the effects of those factors on the high-temperature work-hardening behaviour of metallic materials. In this study, a theoretical discussion was made on the work-hardening behaviour of metallic materials with ellipsoidal second-phase particles at high temperature, based on a micromechanics model developed in the previous study [6] which incorporated the dynamic recovery effect of diffusion of atoms. The micromechanics model in this study is based on the assumption that the misfit strain between ellipsoidal second phase and matrix is uniformly accommodated by diffusion of atoms in the dynamic recovery process. The result of calculations based on this model was then compared with the experimental results by the present authors or other investigators of metallic materials with ellipsoidal second-phase particles.

2. Stress–strain curve at high temperature

2.1. Gibbs free energy and stress–strain curve

It is assumed that the dispersion-hardened metal considered in this study involves N particles of ellipsoidal second phase ($(x_1^2 + x_2^2)/a^2 + x_3^2/c^2 = 1$; volume of a

0022–2461/86 $03.00 + .12

particle: $V = 4\pi a^2 c/3$; aspect ratio of particle: $x = c/a$) with elastic modulus, C^*_{ijkl} (μ^*: rigidity; ν^*: Poisson's ratio), different from that of the matrix, C_{ijkl} (μ: rigidity; ν: Poisson's ratio). The deformation of the material under an applied stress, σ^A_{33} or σ^A_{11}, was considered in this study, because the work-hardening behaviour can depend on the relative orientations of particle habit and applied stress. Suppose that the uniform plastic deformation, $\varepsilon^*_{33} = -2\varepsilon^*_{11} = -2\varepsilon^*_{22} = \varepsilon^*$ (or $\varepsilon^*_{11} = -2\varepsilon^*_{22} = -2\varepsilon^*_{33} = \varepsilon^*$), occurs only in the matrix under an applied stress, σ^A_{33} (or σ^A_{11}). It is also assumed here that second-phase particles do not deform plastically, and that the interaction among the stress fields of particles is negligible because of the small volume fraction of second phase.

According to Tanaka and Mori [1], the Gibbs free energy of the material, G, is expressed with the volume fraction of second phase, $f (= NV/V_0$; where V_0 is the total volume of the material), by the following equation.

$$G = 1/2A\mu\varepsilon^{*2}fV_0 + B\sigma^A\varepsilon^* fV_0 + \sigma_0\varepsilon^* V_0 - \sigma^A\varepsilon^* V_0 + E_0(\sigma^A) \quad (1)$$

where σ^A is an external stress, σ^A_{11} or σ^A_{33}. In the above equation, the first term is the elastic strain energy of the material, and the second term is the interaction energy between external stress and internal stress field. The third and fourth terms are the energy dissipation and the decrease in external potential, respectively, and σ_0 is the yield stress. A and B are shape factors expressed by the Eshelby tensor [2], elastic moduli of the matrix and second phase (C_{ijkl} and C^*_{ijkl}) [7]. $E_0(\sigma^A)$ involves the energy term associated with disturbed external stress field due to the rigidity effect, and is independent of ε^*.

From the equilibrium condition of the system [1], the applied stress, σ^A (σ^A_{11} or σ^A_{33}), is given by

$$\sigma^A = A\mu\varepsilon^* f/(1 - Bf) + \sigma_0/(1 - Bf) \quad (2)$$

The work-hardening rate is expressed as

$$\theta = d\sigma^A/d\varepsilon^* = A\mu f/(1 - Bf) \quad (3)$$

where θ denotes θ_1 or θ_3 (suffix indicates tensile direction, x_1 or x_3). Substituting Equation 2 into Equation 1, we obtain

$$G = -1/2A\mu\varepsilon^{*2}fV_0 + E_0(\sigma^A) \quad (4)$$

The total free energy change is given by $\delta G = -A\mu\varepsilon^* fV_0\delta\varepsilon^*$ when ε^* changes by $\delta\varepsilon^*$ in the deformation of the material. It is obvious in this case that $\delta G = -\delta E_{el}$, since the change in the elastic strain energy, δE_{el}, is expressed by $\delta E_{el} = A\mu\varepsilon^* fV_0\delta\varepsilon^*$. Therefore, the same result as the one which will be given in the following chapters can be obtained, even if the change in the elastic strain energy, δE_{el}, is only considered in the analysis [6].

2.2. Dynamic recovery model

The excess (and deficit) of volume occurs in the matrix around an ellipsoidal second-phase particle as a result of the uniform plastic deformation in the matrix [6]. The geometrical consideration revealed that the excess (or deficit) of volume amounts to $\Delta V \fallingdotseq 3^{\frac{1}{2}}\varepsilon^* V/3$ in this case as well as in the material with spherical second-phase particles in which the uniform plastic strain occurs [6]. ε^* is identical to the engineering plastic strain, ε, when no recovery occurs. The number of atoms, n, involved in ΔV and the corresponding value without recovery, n_0, are respectively given by

$$n = \Delta V/\Omega \fallingdotseq 3^{\frac{1}{2}}\varepsilon^* V/(3\Omega), \quad n_0 \fallingdotseq 3^{\frac{1}{2}}\varepsilon V/(3\Omega) \quad (5)$$

where Ω is the atomic volume of matrix phase. If Equation 4 is rewritten using Equation 5, G is also expressed by

$$G = -3A\mu n^2\Omega^2/(2V) + E_0(\sigma^A) \quad (6)$$

It is considered that the Gibbs free energy of the system decreases by dG when atoms, dn, are emitted from region with excessive volume and are absorbed to that with deficit of volume. The difference in chemical potential between the emission and absorption sides of atoms, $\Delta\mu$, is then given by

$$\Delta\mu = -dG/dn = 3A\mu n\Omega^2/V \quad (7)$$

The flux of atoms, J, in general form is expressed as follows, with the average diffusion distance of atoms, L.

$$J = \frac{D}{\Omega kT}\,\mathrm{grad}\,\Delta\mu = \frac{3A\mu n\Omega D}{kTLV} \quad (8)$$

D, k and T are diffusion coefficient, Boltzmann's constant and absolute temperature, respectively. The emission rate of atoms, $[dn/dt]$, is given by

$$\left[\frac{dn}{dt}\right] \fallingdotseq SJ = \frac{3A\mu n\Omega DS}{kTLV} \quad (9)$$

where S is the total cross section of diffusion. D is D_v (volume diffusion coefficient) for the recovery controlled by volume diffusion of atoms. D should be D_{gb} (grain-boundary diffusion coefficient) when the matrix–particle interface is an incoherent boundary and when the recovery is controlled by grain-boundary diffusion.

In this study, the approximate values of S and L were used in the calculation which were dependent on aspect ratio, x, and orientation of second-phase particle, as shown in Fig. 1, although S and L are considered to be complex functions of them. According to the result of analysis in the previous study [6], L was taken as the average distance from region with excessive volume to that with deficit of volume for both volume diffusion and grain-boundary diffusion of atoms. It was assumed that S for volume diffusion, S_v, was of the order of maximum cross-section of a second-phase particle normal to the direction of atom migration, because a high stress concentration occurred only in the vicinity of it. S for grain-boundary diffusion, S_{gb}, was approximated to be of the order of the maximum cross-section of the particle–matrix interface perpendicular to the direction of atom diffusion.

In tensile deformation, the increase of excess (or deficit) of atoms with time, dn_0/dt, can be defined from Equation 5 corresponding to the plastic strain rate, $\dot{\varepsilon}$ ($= d\varepsilon/dt$). Since excessive atoms are decreased by dn/dt in the recovery process (Equation 9), the total

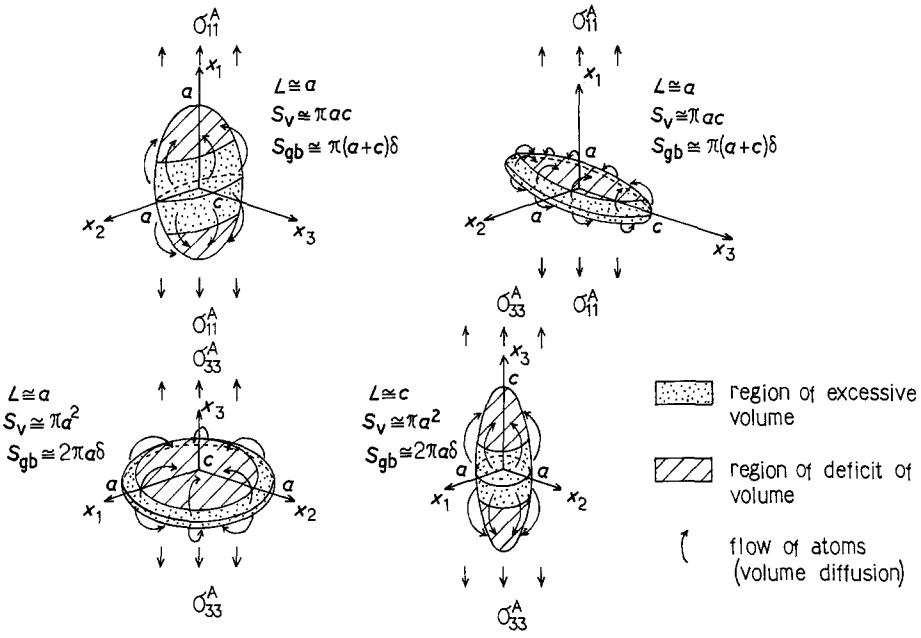

Figure 1 Values of S and L used in the calculation.

migration rate of atoms, dn/dt, is given by

$$dn/dt = dn_0/dt - [dn/dt]$$
$$= \frac{3^{\frac{1}{2}}V\dot{\varepsilon}}{3\Omega} - \frac{3A\mu\Omega DS}{kTLV}n = \bar{B} - Cn \quad (10)$$

where $\bar{B} = 3^{\frac{1}{2}}V\dot{\varepsilon}/(3\Omega)$ and $C = 3A\mu\Omega DS/(kTLV)$. This differential equation of primary reaction has the same form as that of the previous study [6], because the uniform accommodation of the misfit strain is also assumed in this study. C is defined by shape, size and orientation of a second-phase particle and by the recovery process. Table I shows the approximate values of C and L used in the calculation when the volume of a second-phase particle is kept constant (i.e. $V = 4\pi a^2 c/3 = 4\pi a^{*3}/3 = \text{const.}$).

If Equation 10 is solved under the initial condition of $n = 0$ for $t = 0$ when $\dot{\varepsilon}$ is constant, the solution of n is given by

$$n = (\bar{B}/C)\{1 - \exp(-Ct)\}$$
$$= (\bar{B}/C)\{1 - \exp(-C\varepsilon/\dot{\varepsilon})\} \quad (11)$$

Substituting Equation 11 into Equation 4 and rearranging, ε^* is expressed by

$$\varepsilon^* = (\dot{\varepsilon}/C)\{1 - \exp(-C\varepsilon/\dot{\varepsilon})\} \quad (12)$$

The stress–strain curve which incorporates the recovery effect is given by substituting Equation 12 into Equation 2.

$$\sigma^A = \frac{A\mu f}{1 - Bf}\frac{\dot{\varepsilon}}{C}\{1 - \exp(-C\varepsilon/\dot{\varepsilon})\} + \frac{\sigma_0}{1 - Bf} \quad (13)$$

The work-hardening rate in this case is also expressed as

$$\Theta = \frac{d\sigma^A}{d\varepsilon} = \frac{A\mu f}{1 - Bf}\exp(-C\varepsilon/\dot{\varepsilon}) \quad (14)$$

where Θ denotes Θ_1 or Θ_3 (suffix indicates tensile direction, x_1 or x_3).

3. Numerical calculation of work-hardening rate

Figs 2 and 3 show the work-hardening rate against aspect ratio, x, on the material with second-phase particles for $f = 0.05$ and $\varepsilon = 0.01$ (in either case with or without the dynamic recovery). The volume of a second-phase particle was kept constant in this calculation ($4\pi a^2 c/3 = 4\pi a^{*3} = \text{const.}$). The numerical values used in the calculation are $a^* = 5 \times 10^{-8}$ m, $\delta \cong 2b = 5.10 \times 10^{-10}$ m, $D_v = 8.23 \times 10^{-20}$ m^2 sec^{-1} (923 K) [6], $D_{gb} = 1.05 \times 10^{-17}$ m^2 sec^{-1} (723 K) [8], $\Omega = 7.10 \times 10^{-6}$ m^3 mol^{-1}, $\mu = 5.83 \times 10^4$ MPa, $\nu^* = \nu = 0.30$, and $\dot{\varepsilon} = 1.33 \times 10^{-4}$ sec^{-1}. The work-hardening rate in those figures was normalized by dividing the calculated value by the rigidity of matrix, μ. In the absence of dynamic recovery, as indicated by dotted lines in the figures, the work-hardening rate increases with an increase in the ratio of rigidity of second phase to that of matrix phase (rigidity ratio), m ($= \mu^*/\mu$), whereas it has a small value when aspect ratio (x) is close to unity. The work-hardening rate of the material is strongly affected by the dynamic recovery. In the recovery controlled by volume diffusion of atoms, the

TABLE I Values of C used in the calculation

	ε_{ij}^*	$\varepsilon_{33}^* = -2\varepsilon_{11}^* = -2\varepsilon_{22}^* = -\varepsilon^*$			$\varepsilon_{11}^* = -2\varepsilon_{22}^* = -2\varepsilon_{33}^* = -\varepsilon^*$
	x	$x < 1$	$x = 1$	$x > 1$	$x \lesssim 1$
Volume diffusion	$\frac{C/9A\mu\Omega D_v}{4kT}$	$\frac{1}{a^{*2}x^{\frac{1}{2}}}$	$\frac{1}{a^{*2}}$	$\frac{1}{a^{*2}x x^{\frac{1}{2}}}$	$\frac{(x^2)^{\frac{1}{2}}}{a^{*2}}$
Grain-boundary diffusion	$\frac{C/9A\mu\Omega D_{gb}\delta}{2kT}$	$\frac{1}{a^{*3}}$	$\frac{1}{a^{*3}}$	$\frac{1}{a^{*3}x}$	$\frac{1+x}{2a^{*3}}$

δ = grain-boundary thickness ($\cong 2b$, b: magnitude of Burgers vector).

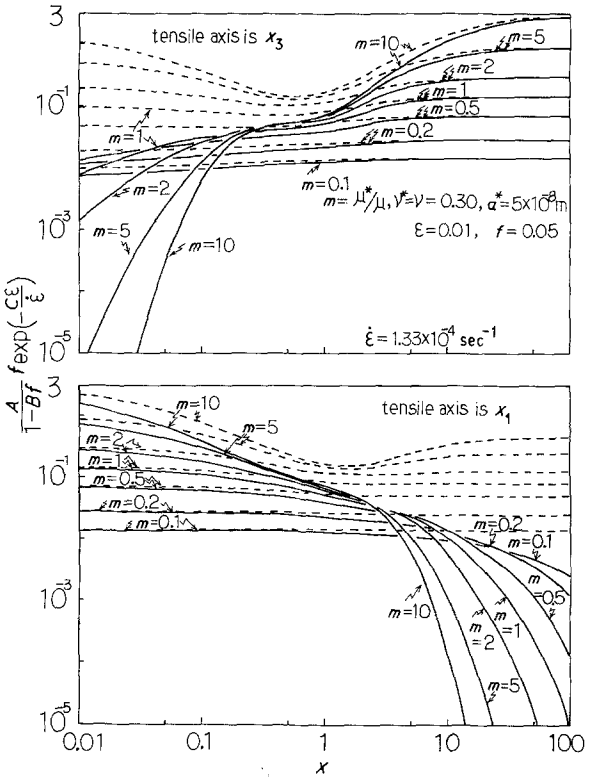

Figure 2 The work-hardening rate against aspect ratio, x, on the material with second-phase particles (the dynamic recovery is controlled by volume diffusion of atoms in this case). (——) Recovery by volume diffusion, (– – –) without recovery.

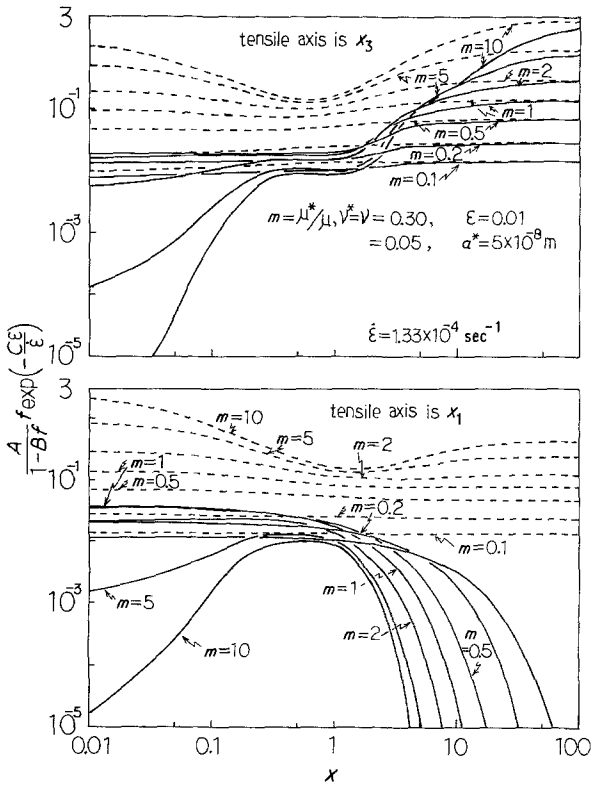

Figure 3 The work-hardening rate against aspect ratio, x, on the material with second-phase particles (the dynamic recovery is controlled by grain-boundary diffusion in this case). (——) Recovery by grain-boundary diffusion, (– – –) without recovery.

work-hardening rate decreases with a decrease of x when x_3 is the tensile axis, and also decreases with an increase of x when x_1 is the tensile direction. The decrease in work-hardening rate is more remarkable with larger values of the rigidity ratio, m (Fig. 2). Further, in the recovery controlled by grain-boundary diffusion, the effect of aspect ratio (x) on the work-hardening rate is somewhat analogous to that with the recovery governed by volume diffusion when x_3 is the tensile axis. The effect of dynamic recovery is relatively small when x_1 is the tensile axis and x is close to unity.

Thus, it is found that the work-hardening behaviour of the material at high temperature depends not only on the aspect ratio, x, the rigidity ratio, m, or the orientation of second phase, but also on the controlling process of recovery. It is also pointed out that a large value of m does not always lead to a large work-hardening rate. This may be attributed to the fact that a large m results in a large elastic strain energy and the dynamic recovery is thereby promoted, and because the volume of a second-phase particle was kept constant in the calculation. It should be noted that the pre-existing strong dislocation structure [9] or the plastic relaxation in the vicinity of second-phase particles [1] can affect the recovery process around particles in the high-temperature deformation.

Fig. 4 shows the effect of particle size of second phase on the work-hardening rate of the material at high temperature. The work-hardening rate decreases with a decrease of particle size from $2a^*$ to $a^*/2$ owing to the enhanced recovery. Further, a large rigidity ratio (m) does not necessarily lead to a large work-hardening rate, because both a change in aspect ratio and a decrease of particle size also affect the dynamic recovery around particles. On the high-temperature deformation of the metallic material with second-phase particles, it was predicted from the results of calculations in this study that the effect of decreasing the particle size is identical to that of decreasing the strain rate, increasing the plastic strain in the matrix, and increasing the deformation temperature on the work-hardening rate, and that those consistently decrease the work-hardening rate of the material with second phase at high temperature.

4. Results of calculation and experiment in high-temperature deformation

A tensile test was performed on austenite 21Cr–4Ni–9Mn steel with rod-like $M_{23}C_6$ carbides, which has almost the same rigidity and Poisson's ratio as those of the matrix phase ($\mu^* = \mu$, $\nu^* = \nu$) [6], under a constant strain rate of $1.33 \times 10^{-4}\,\text{sec}^{-1}$ in the temperature range 306 to 1073 K (33 to 800° C). 21Cr–4Ni–9Mn steel in this study has the basic compositions of 0.51% C, 0.40% N, 20.22% Cr, 3.90% Ni and 8.75% Mn. The steel was directly quenched into a furnace maintained at 1173 K (900° C) and was then aged for 108×10^3 sec (30 h) to develop 10 vol % rod-like $M_{23}C_6$ carbides ($a = 5.55 \times 10^{-8}$ m).

Fig. 5 shows the work-hardening rate at $\varepsilon = 0.01$ in the rapid hardening region against test temperature. A considerable contribution of solid-solution hardening can be expected in this steel with a large amount of carbon and nitrogen. This contribution at elevated temperature, $(\theta_{sol})_T$, was then calculated for aged steel

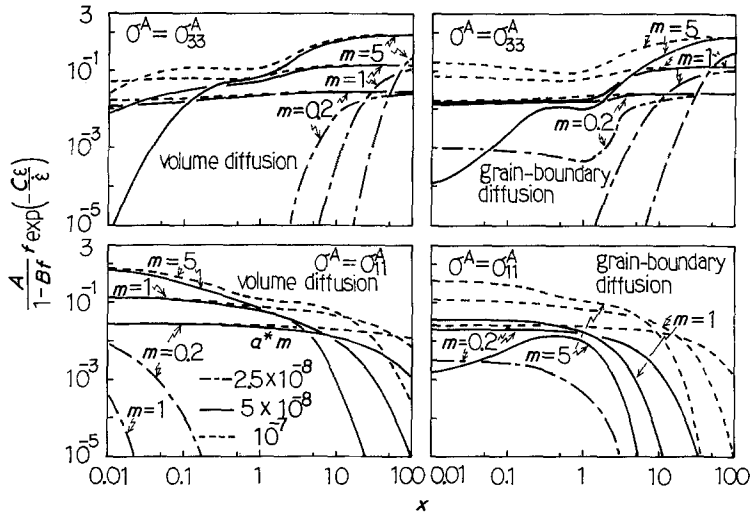

Figure 4 Effect of particle size on the work-hardening rate of the material with second-phase particles at high temperature ($m = \mu^*/\mu$, $\nu^* = \nu = 0.30$, $f = 0.05$, $\varepsilon = 0.01$ and $\dot{\varepsilon} = 1.33 \times 10^{-4}\,\mathrm{sec}^{-1}$).

using the following equation [6]:

$$(\theta_{sol})_T = 5970 \left(\frac{\mu_T}{\mu_{RT}}\right)\left(\frac{c_T}{c_0}\right)^{1/2} \text{(MPa)} \qquad (15)$$

when μ_{RT} and μ_T are the rigidity of matrix phase at room temperature and at elevated temperature, respectively. The rigidity and Poisson's ratio of AISI316 steel at elevated temperature were used in the calculations in this study [10], because those values are still unknown in 21Cr–4Ni–9Mn steel. c_0 and c_T are the concentration of solute atoms dissolved in the matrix for solid solution and for aged steel, respectively. $c_0 = 3.91$ at % and $c_T = 1.30$ at % were obtained by dint of X-ray analysis [11]. The result of calculations using Equation 15 is also shown in Fig. 5.

Fig. 6 shows the temperature dependence of the net work-hardening rate due only to the presence of rod-like $M_{23}C_6$ carbides and that of the calculated value. The experimental and calculated values previously obtained for the material with spherical $M_{23}C_6$ carbides [6] are also shown in this figure. The experimental value in the figure was obtained by subtracting the contribution of solid-solution hardening, calculated from Equation 15, from the experimental result and then being temperature-compensated. The decrease in the work-hardening rate due to dynamic recovery occurs at higher temperature in the material with rod-like $M_{23}C_6$ carbides ($x = 10$, $a = 5.55 \times 10^{-8}$ m) than in that with spherical $M_{23}C_6$ carbides ($x = 1$, $a = 5.3 \times 10^{-8}$ m). It was assumed in this calculation that the dynamic recovery is controlled by volume diffusion of atoms. Other physical constants used are $D_v = 1.8 \times 10^{-5} \exp(-253\,\mathrm{kJ\,mol^{-1}}/RT)\mathrm{m^2\,sec^{-1}}$ [6], $b = 2.55 \times 10^{-10}$ m [6], and $\Omega = 7.10 \times 10^{-6}\,\mathrm{m^3\,mol^{-1}}$ [6]. The calculated value from Equation 14 (Θ_1 or Θ_3) was normalized by the value without recovery (θ_1 or θ_3) (Equation 3), namely, $\bar{\Theta}_1 = \Theta_1/\theta_1$ and $\bar{\Theta}_3 = \theta_3/\theta_3$. The experimental data lie between the calculated values, where the tensile directions are x_1 ($\bar{\Theta}_1$) and x_3 ($\bar{\Theta}_3$), respectively. Then, the orientation of second-phase particle was taken into account, provided that one-third of the carbides lie in parallel with the tensile axis (Θ_3) and the rest are normal to the tensile axis (Θ_1). The average work-hardening rate is given by $\Theta_{av} = (\Theta_3 + 2\Theta_1)/3$. The corresponding value without recovery is expressed as $\theta_{av} = (\theta_3 + 2\theta_1)/3$. The normalized value, $\bar{\Theta}$ ($= \Theta_{av}/\theta_{av}$), is also shown in Fig. 6. This value is very close to the experimental one, while it is somewhat larger than that observed in the high-temperature range.

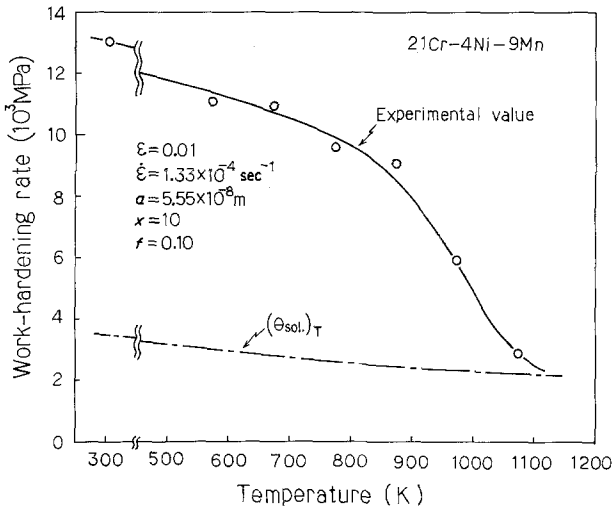

Figure 5 The work-hardening rate against temperature on austenitic 21Cr–4Ni–9Mn steel with rod-like $M_{23}C_6$ carbides.

Fig. 7 shows the calculated and experimental stress–strain curves after yielding of an aged 21Cr–4Ni–9Mn steel with rod-like $M_{23}C_6$ carbides. The orientation of second-phase particle was also taken into account in the calculation, assuming that the averaged stress is given by $(\sigma_{33}^A + 2\sigma_{11}^A)/3$. The contribution of solid-solution hardening to the work-hardening rate of the material was estimated by the following equation [6]:

$$\sigma_s = \frac{\mu_T}{\mu_{RT}}\left(\frac{c_T}{c_0}\right)^{1/2}(940\varepsilon^{0.066} - 564)\ \text{(MPa)}$$

$$(\varepsilon \geqq 0.0005) \qquad (16)$$

The calculated value shown in the figure also involves the contribution of solid-solution hardening, σ_0, estimated from Equation 16. A good correlation is found between the result of calculation and that of experiment in this material up to small plastic strain below

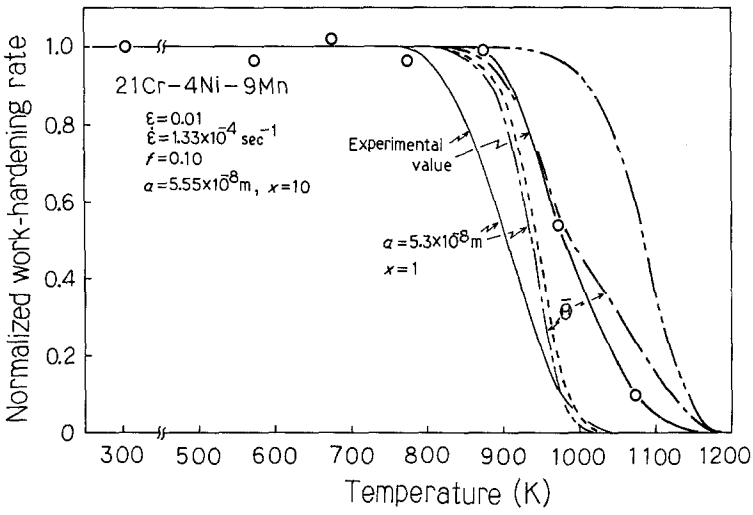

Figure 6 The normalized work-hardening rate by calculation and the one of experiment on austenitic 21Cr–4Ni–9Mn steel with rod-like $M_{23}C_6$ carbides. (○) Experimental value. Calculated value; (——) $\bar{\Theta}_1$, (— — —) $\bar{\Theta}_2$, (— — —) $\bar{\Theta}_{e3}$.

about 0.01, but the calculated stress is higher than the experimental value, especially at larger plastic strain and lower temperature. This discrepancy may be attributed to the fact that the model used in this study does not involve the effect of another recovery process such as plastic accommodation around second-phase particles [1]. The model would be applicable up to higher strain in the material deformed at lower strain rate, because more rapid diffusional recovery might be expected to delay the onset of plastic relaxation.

Fig. 8 shows the calculated and experimental stress–strain curves after yielding of aluminium containing 3.03 vol % Al_2O_3 (SAP) ($a = 3.2 \times 10^{-8}$ m, $x = 0.3$) in the tensile deformation [9, 12]. It was assumed in the calculation that the dynamic recovery is controlled by grain-boundary diffusion at 293 K (20° C), while it is governed by volume diffusion at 473 K (200° C). The physical constants used are $\mu = 25.9$ GPa (293 K), 23.4 GPa (473 K) [13], $\nu = 0.35$ (293 K, 473 K) [13], $\mu^* = 149$ GPa (293 K), 147 GPa (473 K) (those values were calculated from the data given by Muramatsu [13] and Shiraki [14]), $D_v = 3.5 \times 10^{-6} \exp(-120.3\,\text{kJ mol}^{-1}/RT)\text{m}^2\text{sec}^{-1}$ [4], $D_{gb} = D_p = 10^{-6} \exp(-66.9\,\text{kJ mol}^{-1}/RT)\text{m}^2\text{sec}^{-1}$ [4], $\Omega = 10.03 = 10^{-6}\text{m}^3\text{mol}^{-1}$ [15] and $b = 2.70 \times 10^{-10}$ m [15]. Poisson's ratio of the second phase was assumed to be the same as that of matrix phase ($\nu^* = \nu$). The orientation of second-phase particle was also taken into account as before, assuming that one-third of Al_2O_3 particles have their broad surfaces normal to tensile axis (σ_{33}^A) and the rest have the surfaces in parallel with tensile axis (σ_{11}^A). Further, the strength of pure aluminium was also added to the calculated value [9]. The result of the calculation agrees well with that of experiment for small plastic strain below about 0.01 both at 293 and 473 K. This may imply that the recovery process is governed by dislocation climbing at the matrix–particle interface at 293 K, while it is controlled by climbing of dislocation in the matrix at 473 K.

As is known from the above result, a good correlation was found between the result of calculation and that of experiment in metallic materials with ellipsoidal second-phase particles. The assumption that the misfit at the interface of second-phase particles would be uniformly accommodated by diffusion of

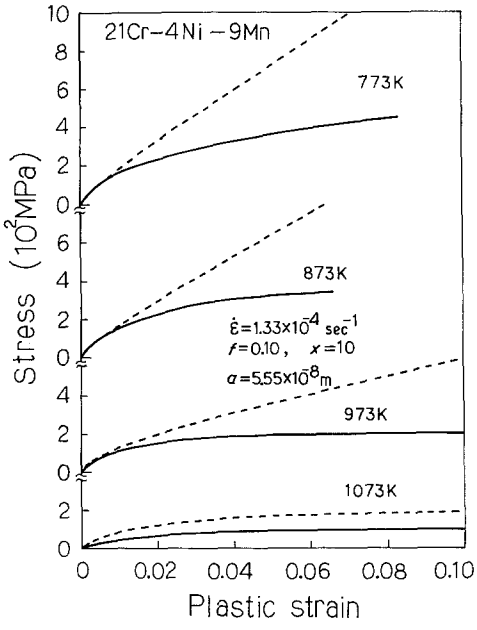

Figure 7 The calculated stress–strain curve after yielding and that obtained by experiment on austenitic 21Cr–4Ni–9Mn steel with rod-like $M_{23}C_6$ carbides. (——) Experimental and (— — —) calculated values.

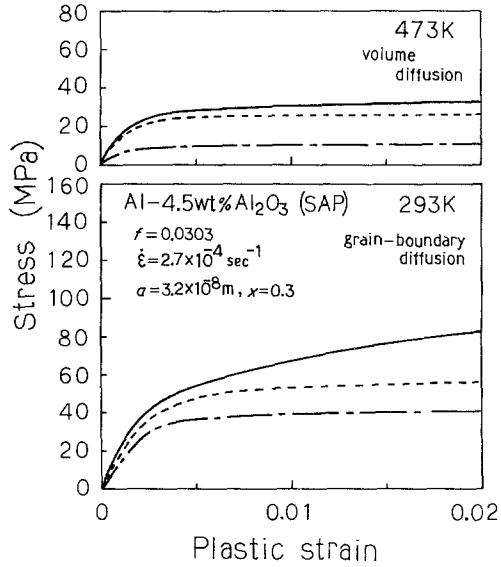

Figure 8 Stress–strain curve after yield on SAP. (——) Experimental value, (— — —) pure aluminium, (— — —) calculated value.

atoms, seems to be almost satisfied in the dynamic recovery process. The dynamic recovery model used in this study involves no ambiguous parameters, and therefore, the high-temperature deformation of metallic materials with second-phase particles can be calculated using the physical constants including the rigidity and Poisson's ratio of the second phase and those of the matrix phase, and the diffusion coefficient, if only shape, size and volume fraction of the particles are known. Further, it is also possible to know the controlling mechanism of the dynamic recovery by comparing the calculated value based on the micromechanics model with the experimental result.

5. Conclusion

The high-temperature work-hardening behaviour of the metallic material containing ellipsoidal second-phase particles has been analysed using a continuum mechanics model which incorporated the dynamic recovery controlled by volume diffusion or grain-boundary diffusion of atoms. A reasonable correlation was found between the result of calculation based on the model and that of experiment on metallic materials up to a plastic strain below about 0.01, but the calculated stress is higher than the observed stress at larger plastic strain and lower temperature, because the model does not include any other recovery processes.

The dynamic recovery model in this study does not involve any ambiguous parameters. Therefore, one can calculate the work-hardening behaviour of the material at high temperature, using only physical constants including shape, size and volume fraction of second phase, elastic moduli of second phase and matrix, and the diffusion coefficient. The present model is applicable to the understanding of high-temperature deformation behaviour or to the prediction of the possible recovery mechanism of metallic materials with ellipsoidal second-phase particles.

Acknowledgement

We wish to thank Associate Professor, T. Sakaki, of Faculty of Technology, Tokyo Metropolitan University, for his helpful advice on the calculation in this study.

References

1. K. TANAKA and T. MORI, *Acta Metall.* **18** (1970) 931.
2. J. D. ESHELBY, *Proc. R. Soc. Ser. A* **241** (1957) 376.
3. T. MORI and H. TOKUSHIGE, *Acta Metall.* **25** (1977) 635.
4. K. MATSUURA, *J. Jpn. Inst. Metals* **44** (1980) 346.
5. M. F. ASHBY, Proceedings 2nd International Conference on Strength of Metals and Alloys, Vol. II (American Society for Metals, Asilomar, 1970) p. 534.
6. M. TANAKA and H. IIZUKA, *J. Mater. Sci.* **19** (1984) 3976.
7. K. TANAKA, K. WAKASHIMA and T. MORI, *J. Mech. Phys. Solids* **21** (1973) 207.
8. W. BEERE and M. V. SPEIGHT, *Met. Sci.* **12** (1978) 593.
9. E. RUEDL and P. GUYOT, in "Modern Developments in Powder Metallurgy", Vol. 2 (Plenum, New York, 1966) p. 131.
10. A. MURAMATSU, *J. Jpn. Soc. Mech. Eng.* **68** (1965) 1623.
11. M. TANAKA, O. MIYAGAWA and D. FUJISHIRO, *J. Jpn. Inst. Metals* **41** (1977) 11.
12. P. GUYOT, in "Modern Developments in Powder Metallurgy", Vol. 2 (Plenum, 1966) p. 112.
13. A. MURAMATSU, "Elastic Modulus of Metallic Materials" (Japan Society of Mechanical Engineers, Tokyo, 1980) p. 159.
14. Y. SHIRAKI, "Ceramics Manual" (Gihoudo Press, Tokyo, 1982) p. 508.
15. S. KODA, "Introduction to Metal Physics" (Corona, Tokyo, 1978) p. 45.

Received 2 April
and accepted 15 July 1985